Boundary-layer receptivity for a parabolic leading edge. Part 2. The small Strouhal number limit.

By P. W. HAMMERTON † AND E. J. KERSCHEN

Department of Aerospace & Mechanical Engineering, University of Arizona, Tucson, AZ 85721, USA

(Received 4 June 1996 and in revised form 2 August 1997)

In Hammerton & Kerschen (1996), the effect of the nose radius of a body on boundary-layer receptivity was analysed for the case of a symmetric mean flow past a two-dimensional body with a parabolic leading edge. A low Mach number two-dimensional flow was considered. The radius of curvature of the leading edge, r_n, enters the theory through a Strouhal number, $S = \omega r_n/U$, where ω is the frequency of the unsteady free-stream disturbance and U is the mean flow speed. Numerical results revealed that the variation of receptivity for small S was very different for free-stream acoustic waves propagating parallel to the mean flow and those free-stream waves propagating at an angle to the mean flow. In this paper the small-S asymptotic theory is presented. For free-stream acoustic waves propagating parallel to the symmetric mean flow, the receptivity is found to vary linearly with S, giving a small increase in the amplitude of the receptivity coefficient for small S, compared to the flat plate value. In contrast, for oblique free-stream acoustic waves, the receptivity varies with $S^{\frac{1}{2}}$, leading to a sharp decrease in the amplitude of the receptivity coefficient, relative to the flat plate value. Comparison of the asymptotic theory with numerical results obtained in the earlier paper confirms the asymptotic results but reveals that the numerical results diverge from the asymptotic result for unexpectedly small values of S.

1. Introduction

The receptivity process through which free-stream disturbances generate instability waves in boundary layers generally comes about through non-parallel mean flow effects, which may arise either in the leading-edge region, or in a localized region farther downstream in the boundary layer (Goldstein & Hultgren 1989; Kerschen 1990).

In Goldstein (1983), an asymptotic analysis was developed for leading-edge receptivity on a semi-infinite zero-thickness plate. Leading-edge receptivity coefficients for various free-stream disturbances were calculated by Goldstein, Sockol & Sanz (1983) and Heinrich & Kerschen (1989). However, aerodynamic bodies designed for subsonic flow generally have finite thickness distributions with a parabolic leading edge. In Hammerton & Kerschen (1996) (hereafter referred to as HK1), the influence of the thickness of a body was examined. The situation considered was a thin, symmetric airfoil of chord $2b$ at zero angle-of-attack in a uniform flow of speed U. A plane acoustic wave of frequency ω, propagating at an angle θ with respect to the airfoil chord, was assumed to be incident

† Present address: School of Mathematics, University of East Anglia, Norwich, NR4 7TJ, UK

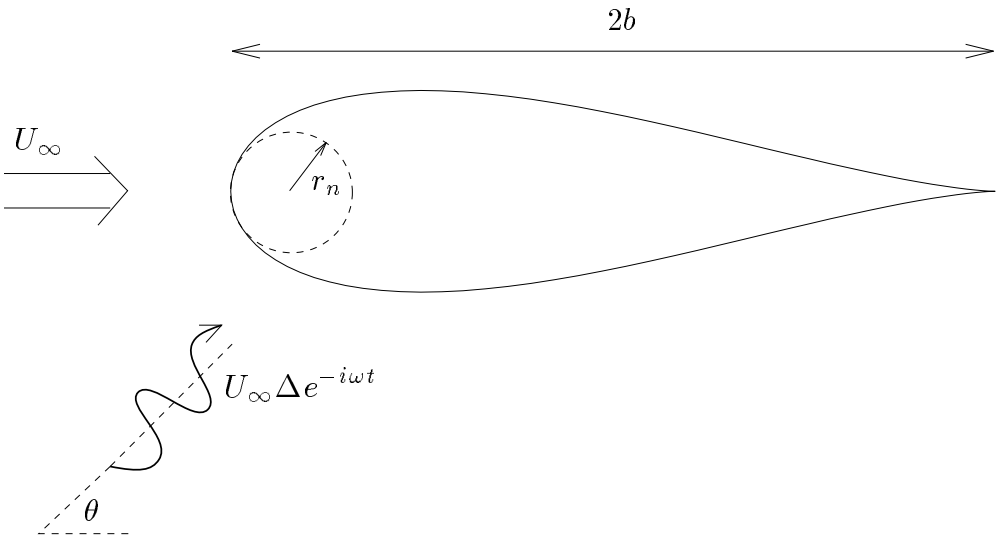

FIGURE 1. An illustration of the physical situation of interest: a thin, symmetric airfoil of chord $2b$ is at zero angle-of-attack in a uniform flow of speed U, with a plane acoustic wave incident at an angle θ with respect to the airfoil chord.

on the airfoil as illustrated in figure 1. A high Reynolds number asymptotic analysis ($\epsilon^6 = \nu\omega/U^2$; $\epsilon \ll 1$) was formulated for an incompressible, two-dimensional flow. The nose radius of the leading edge, r_n, enters through a Strouhal number,

$$S = \frac{\omega r_n}{U} \tag{1.1}$$

which is the ratio of the nose radius and the hydrodynamic length scale, U/ω.

When $S = O(1)$, two streamwise regions enter the analysis, one region where the distance downstream is $O(U/\omega)$ and the disturbance is governed by the linearised unsteady boundary layer equation (LUBLE), and a second region at distances $O(\epsilon^{-2}U/\omega)$ where the disturbance is governed by the triple-deck structure, corresponding to the asymptotic form of the Orr–Sommerfeld equation (OSE) in the vicinity of the lower branch. In the LUBLE region, the inviscid pressure field and slip velocity induced by the free-stream disturbance drives the unsteady motion in the boundary layer. Far downstream in the LUBLE region, the solution consists of a generalised Stokes wave, and a set of asymptotic eigensolutions. The wavelengths of these eigenfunctions shorten progressively with distance downstream. Eventually, the self-induced pressure field associated with the displacement thickness of each asymptotic eigenfunction becomes significant, and the triple-deck structure replaces the LUBLE as the correct asymptotic approximation to the Navier–Stokes equation. It can be shown that the first asymptotic eigenfunction of the LUBLE matches on to the Tollmien–Schlichting wave solution of this triple-deck region. Thus, the form of the free-stream disturbance and the geometry close to the nose influence the amplitude of the Tollmien–Schlichting wave only through the coefficient C_1 of the first asymptotic eigenfunction. Therefore, we call C_1 the 'receptivity coefficient'. The asymptotic analysis far downstream in the LUBLE region determined the form of

the eigenfunctions, but not their coefficients C_i. These coefficients can be found only through a full solution of the LUBLE, which must be determined by numerical methods.

Theory for $S = O(1)$ was developed in HK1, where associated numerical results were also presented. These results showed that the receptivity associated with a symmetric free-stream disturbance increases slightly with S, for small S (HK1, figure 4*a*), but the receptivity associated with a free-stream disturbance that is anti-symmetric about the leading edge decreases sharply with S (HK1, figure 5*a*). In the present paper, a small-S asymptotic theory is developed. In this limit, the streamwise development of the boundary layer can be divided into three regimes. In the nose region, where the distance downstream is $O(r_n)$, the unsteady motion in the boundary layer is quasi-steady at leading order. In the LUBLE region, where the downstream distance is $O(U/\omega)$, the unsteady terms enter at leading order in the disturbance equations, but the mean pressure gradient is small so that the mean boundary layer flow approaches the flat-plate solution. In the OSE region further still downstream, a triple-deck structure arises as before. In the small-S asymptotic analysis presented in this paper, we focus on the nose and LUBLE regions. The subsequent asymptotic matching to the OSE region follows that discussed in HK1. Our analysis involves two small parameters, S and ϵ. Formally, we take $\epsilon \to 0$ and then consider the small-S limit, obtaining correction terms of $O(S^{1/2}, S)$. We require the boundary-layer approximation to be valid in the nose region $x_d = O(r_n)$, which is true if the Reynolds number based on nose radius is large,

$$\frac{U r_n}{\nu} = \frac{S}{\epsilon^6} \gg 1. \tag{1.2}$$

This condition is also equivalent to the requirement that the perturbation in the receptivity coefficient due to finite Reynolds number is smaller than that due to geometric effects. Thus the asymptotic theory is more relevant to the limit $\omega \to 0$ rather than $r_n \to 0$.

In §2, the equations governing the mean flow and the time dependent perturbation in the boundary layer are obtained. The small-S asymptotic structure of the unsteady flow in the boundary layer, produced by the symmetric and anti-symmetric components of the free-stream disturbance, is analysed in §§3 and 4 respectively. In §5, numerical solutions of the asymptotic equations are presented, and the resulting asymptotic expressions for the receptivity coefficient are compared with the numerical results of HK1. Finally in §6, the results are summarised and brief comparisons with experiments are made.

2. Formulation

Full details of the derivation of the equations governing the boundary layer flow are given in HK1, together with interpretation of the evolution of the unsteady disturbances that eventually lead to instability. Here we provide only the key equations necessary to illustrate the small Strouhal number limit which is the subject of the present paper.

The streamfunction Ψ in the boundary layer, non-dimensionalised by the quantity $U\nu^{\frac{1}{2}}/\omega^{\frac{1}{2}}$, is expressed in the form

$$\Psi = \xi\phi + \psi e^{-it} \tag{2.1}$$

where the unsteady component ψ is assumed small compared to the mean flow component $\xi\phi$. We use parabolic coordinates (ξ, η) defined by

$$x_d + iy_d = \frac{1}{2}\frac{U}{\omega}\left(\left[\xi + i(S^{1/2} + \epsilon^3\eta)\right]^2 + S\right), \tag{2.2}$$

where x_d, y_d are (dimensional) cartesian coordinates centred on the airfoil leading edge. The parabolic coordinate ξ along the airfoil surface has been nondimensionalised by the square root of the disturbance length U/ω. For the parabolic coordinate η in the normal direction, the origin has been shifted to the airfoil surface, and the additional factor ϵ^3 in (2.2) corresponds to nondimensionalisation by the quantity $(\nu/U)^{\frac{1}{2}}$. Thus η corresponds to the conventional normal coordinate for the mean boundary layer.

2.1. *Steady flow*

The steady boundary-layer flow is most naturally expressed in terms of a streamwise variable scaled on the nose radius,

$$\bar{\xi} = \xi / S^{1/2}. \tag{2.3}$$

The function $\phi(\bar{\xi}, \eta)$ describing the steady boundary-layer flow then satisfies the differential equation

$$\phi_{\eta\eta\eta} + \phi_{\eta\eta}\phi + \bar{\xi}(\phi_{\eta\eta}\phi_{\bar{\xi}} - \phi_\eta \phi_{\eta\bar{\xi}}) - \frac{1}{1+\bar{\xi}^2}({\phi_\eta}^2 - 1) = 0, \tag{2.4}$$

with boundary conditions

$$\phi = \phi_\eta = 0 \quad \text{at} \quad \eta = 0 \qquad \text{and} \qquad \phi_\eta \to 1 \quad \text{exponentially as} \quad \eta \to \infty. \tag{2.5}$$

For large $\bar{\xi}$, ϕ takes the form (Van Dyke, 1964)

$$\phi(\bar{\xi}, \eta) \sim F(\eta) + \overline{G}_1(\eta)\frac{\ln \bar{\xi}^2}{\bar{\xi}^2} + \overline{G}_2(\eta)\frac{1}{\bar{\xi}^2} + O\left(\frac{1}{\bar{\xi}^{\gamma_2}}\right), \qquad \gamma_2 \approx 3.774, \tag{2.6}$$

where the order of the next higher order term is discussed below. In this expansion, $F(\eta)$ is the Blasius function, and the functions $\overline{G}_i(\eta)$ satisfy homogeneous boundary conditions

$$\overline{G}_i(0) = \overline{G}_i'(0) = 0, \qquad \overline{G}_i' \to 0 \quad \text{exponentially as} \quad \eta \to \infty, \tag{2.7}$$

with governing equations

$$\mathcal{G}_2(\overline{G}_1) = 0, \qquad \mathcal{G}_2(\overline{G}_2) = {F'}^2 - 1 + 2(F''\overline{G}_1 - F'\overline{G}_1'), \tag{2.8}$$

where we define the set of operators $\mathcal{G}_\gamma$ by

$$\mathcal{G}_\gamma(f) \equiv f''' + Ff'' + \gamma F' f' + (1-\gamma)F'' f. \tag{2.9}$$

In the first perturbation term of the large-$\bar{\xi}$ expansion we have $\overline{G}_1 = A_1 G_1$, where

$$G_1 = \eta F'(\eta) - F(\eta), \tag{2.10}$$

which arises as an eigenfunction of $\mathcal{G}_\gamma$ for $\gamma = 2$. The coefficient A_1 remains undetermined at this order. However, the equation for $\overline{G}_2(\eta)$ then takes the form

$$\mathcal{G}_2(\overline{G}_2) = {F'}^2 - 1 + 2A_1 FF''. \tag{2.11}$$

Since the Blasius function F is the solution to the adjoint of $\mathcal{G}_2$, the value of A_1 is fixed by the solvability condition for $\overline{G}_2(\eta)$ which leads to

$$\int_0^\infty F({F'}^2 - 1 + 2A_1 FF'')d\eta = 0, \tag{2.12}$$

and gives $A_1 = 0.60115$.

The equation for $\overline{G}_2(\eta)$ involves the same operator $\mathcal{G}_2$ and hence contains the same eigenfunction. Thus, $\overline{G}_2 = B_1 G_1 + G_2$, where $G_2(\eta)$ satisfies (2.11), with boundary

conditions (2.7) and $G_2''(0) = 0$. Since $\bar{\xi}^{-2}G_1$ is an eigensolution of the boundary-layer perturbation equation, the value of the coefficient B_1 appearing in the $O(\bar{\xi}^{-2})$ term can not be determined by the large-ξ analysis and therefore depends on conditions close to the nose of the body. Numerical integration of (2.4) from $\bar{\xi} = 0$ gives $B_1 \approx 2.08$ (HK1). For all $\gamma > 0$, $\mathcal{G}_\gamma$ has solutions which decay algebraically as $\eta \to \infty$, but only for certain γ do solutions exist which decay exponentially at infinity. Libby & Fox (1963) give the first 10 eigenvalues. The first such eigenvalue, $\gamma_1 = 2$ has already been discussed. The next eigenvalue, $\gamma_2 \approx 3.774$, leads to the next higher order term in the large-$\bar{\xi}$ expansion (2.6).

2.2. *Unsteady flow*

The time-dependent contribution to the boundary-layer flow satisfies the linearised unsteady boundary layer equation (LUBLE),

$$\left.\begin{aligned} \mathcal{F}(\psi) &= (S+\xi^2)^{1/2}\left[\left(i(S+\xi^2) - \frac{S}{S+\xi^2}\right)u_s - \xi\frac{\partial u_s}{\partial \xi}\right], \\ \mathcal{F}(\psi) \equiv \psi_{\eta\eta\eta} + [\phi + \xi\phi_\xi]\psi_{\eta\eta} &+ \left[i(S+\xi^2) - \xi\phi_{\eta\xi} - \frac{S-\xi^2}{S+\xi^2}\phi_\eta\right]\psi_\eta \\ &+ \xi(\phi_{\eta\eta}\psi_\xi - \phi_\eta\psi_{\eta\xi}), \end{aligned}\right\} \tag{2.13}$$

with boundary conditions

$$\psi = \psi_\eta = 0 \quad \text{at} \quad \eta = 0 \qquad \text{and} \qquad \psi_\eta \to (S+\xi^2)^{1/2}\, u_s \quad \text{as} \quad \eta \to \infty. \tag{2.14}$$

Here, $u_s(\xi)$ is the slip velocity induced on the outer edge of the boundary layer by the free-stream disturbance. Note that this equation is written in terms of ξ, the streamwise coordinate scaled on the disturbance length scale U/ω, and hence ϕ must be expressed in terms of ξ.

The development of the solution ψ is described in detail in HK1. Far downstream ($\xi \gg 1$), ψ consists of a particular solution, ψ_p, driven by the local value of the unsteady pressure gradient, together with an infinite set of asymptotic eigensolutions,

$$\psi(\eta, \xi; S) = \psi_p(\eta, \xi; S) + \sum_i C_i(S)\psi_i(\eta, \xi; S). \tag{2.15}$$

The eigensolutions, ψ_i, depend on the geometry of the body far downstream, but are independent of the local free-stream disturbance. In this paper, where we are concerned with the generation of instability waves in the boundary layer, we consider eigensolutions which are generalised forms of the Lam & Rott (1960) eigenfunctions. Another set of eigensolutions could also be calculated, corresponding to generalisations of the functions derived by Brown & Stewartson (1973) for a flat plate. The role of these two sets of eigensolutions is discussed in HK1. The coefficients C_i multiplying the asymptotic eigenfunctions are determined entirely by conditions close to the leading edge ($\xi = O(1)$). One of these eigensolutions, which we label ψ_1, matches on to the Tollmien–Schlichting wave in the Orr–Sommerfeld region farther downstream, where $\xi = O(\epsilon^{-1})$. Thus, it is only through the coefficient C_1 that the unsteady disturbances in the free stream influence the amplitude of the Tollmien–Schlichting wave. Our primary interest is in the relationship between the free-stream disturbances and the amplitude of the Tollmien–Schlichting wave, as a function of Strouhal number S. Thus, we focus on the asymptotic eigensolutions of the LUBLE, which develop a two-layer structure for $\xi \gg 1$. From HK1 (equations 3.17, 3.34, 3.35), at the outer edge of the boundary layer ($\eta \to \infty$), the

first asymptotic eigenfunction takes the form

$$\left.\begin{aligned} \psi_1 &\sim \xi\left(\tfrac{\xi^2}{2}\right)^{\tau_1^{(0)}+S\tau_1^{(1)}} \exp\left(T_1^{(0)}\right)\left(1+O(\xi^{-0.774})\right), \\ \tau_1^{(0)} &= -0.69213, \qquad \tau_1^{(1)} = -1.9878\,\mathrm{i}, \\ T_1^{(0)}(\xi) &= -\lambda\xi^3\left\{\tfrac{1}{3} - A_1 S\frac{\ln(\xi^2/S)}{\xi^2} + (2A_1+\tfrac{3}{2}-B_1)\frac{S}{\xi^2}\right\} \end{aligned}\right\} \tag{2.16}$$

where $\lambda = \mathrm{e}^{-\frac{1}{4}\mathrm{i}\pi}/(\rho_1^{3/2}U_0')$. Here $\rho_1 \approx 1.0187$, the first root of $\mathrm{Ai}'(-\rho)=0$, and $U_0' \equiv F''(0) \approx 0.4696$. The numerical constants A_1 and B_1 arise from the asymptotic form of the mean boundary-layer flow far downstream, (2.6).

For a low Mach number flow, outside the boundary layer the unsteady flow in the vicinity of the leading edge is incompressible and irrotational. Potential flow theory then shows that this local flow consists of symmetric and antisymmetric components of the form

$$u_s(\xi) = \kappa_s\frac{\xi}{(S+\xi^2)^{1/2}} + \kappa_a\frac{1}{(S+\xi^2)^{1/2}}. \tag{2.17}$$

Here $\xi/(S+\xi^2)^{1/2}$ and $1/(S+\xi^2)^{1/2}$ correspond to purely symmetric and anti-symmetric flow about the leading edge, respectively. The coefficients $\kappa_s(\theta)$ and $\kappa_a(\theta)$ multiplying the symmetric and antisymmetric components are independent of the nose geometry, but depend on the free-stream disturbance, being determined by global features of the unsteady flow. When the unsteady disturbance velocity is parallel to the mean flow, (i.e. $\theta = 0$), the forcing is entirely symmetric and $\kappa_s = 0$. For oblique ($\theta \neq 0$) disturbances, the unsteady flow will have both symmetric and anti-symmetric components. Calculation of the coefficients κ_s and κ_a for different free-stream disturbances is discussed in §4 of HK1. Writing $\psi = \kappa_s\psi_s + \kappa_a\psi_a$, and substituting into (2.13), it follows that the receptivity coefficient can be decomposed into contributions from the symmetric and anti-symmetric components of the unsteady outer flow,

$$C_1(S) = \kappa_s\, C_s(S) + \kappa_a\, C_a(S), \tag{2.18}$$

where C_s and C_a are obtained from the solutions of

$$\mathcal{F}(\psi_s) = \xi\left(\mathrm{i}(S+\xi^2) - \frac{2S}{S+\xi^2}\right), \tag{2.19a}$$

$$\mathcal{F}(\psi_a) = \ \mathrm{i}(S+\xi^2) - \frac{S-\xi^2}{S+\xi^2}, \tag{2.19b}$$

respectively. The numerical methods used to obtain values of $C_a(S)$ and $C_s(S)$ for fixed S are described in HK1. The remainder of this paper is concerned with the asymptotic expansions of $C_a(S)$ and $C_s(S)$ as $S \to 0$.

In the nose region, $\bar{\xi} = O(1)$, the mean pressure gradient decreases with distance downstream, and the mean flow approaches the flat-plate limit as $\bar{\xi} \to \infty$. In the small-S limit, the nose-region is quasi-steady at leading order; the linearised boundary layer equations only become fully unsteady when $\xi = O(1)$, i.e. $\bar{\xi} = O(S^{-\frac{1}{2}})$. Thus in the receptivity region $\xi = O(1)$, the mean flow is close to the Blasius solution, and the receptivity coefficient is calculated as a perturbation away from the flat-plate value. Receptivity to the symmetric and anti-symmetric components of the unsteady free-stream disturbance is analysed in §§3 and 4, respectively. In each case the solutions in the nose and receptivity regions are asymptotically matched, and then the large-ξ behaviour in

the receptivity region is compared to (2.16) in order to extract the receptivity coefficient, C_s or C_a.

3. Receptivity to symmetric forcing

For symmetric forcing, (2.19a) suggests that for small S the unsteady perturbation in the nose region, $\bar{\xi} = O(1)$, is quasi-steady at leading order and takes the form

$$\psi_s = S^{\frac{1}{2}}\bar{\xi}\left(\theta_0(\bar{\xi},\eta) + S\,\theta_1(\bar{\xi},\eta) + O(S^2)\right), \tag{3.1}$$

where the functions θ_0 and θ_1 satisfy

$$\left.\begin{aligned} \mathcal{M}_s(\theta_0) &= -\frac{2}{1+\bar{\xi}^2}, \\ \mathcal{M}_s(\theta_1) &= \mathrm{i}(1+\bar{\xi}^2)\big(1-(\theta_0)_\eta\big), \end{aligned}\right\} \tag{3.2}$$

and

$$\mathcal{M}_s(p) \equiv p_{\eta\eta\eta} + (\phi + \bar{\xi}\phi_{\bar{\xi}})p_{\eta\eta} + \left(-\bar{\xi}\phi_{\eta\bar{\xi}} - \frac{2}{1+\bar{\xi}^2}\phi_\eta\right)p_\eta + \phi_{\eta\eta}p + \bar{\xi}(\phi_{\eta\eta}p_{\bar{\xi}} - \phi_\eta p_{\eta\bar{\xi}}). \tag{3.3}$$

The factor $S^{\frac{1}{2}}\bar{\xi}$ is extracted from ψ_s in (3.1) to simplify the boundary conditions, which become

$$\left.\begin{aligned} \theta_0 = \frac{\partial\theta_0}{\partial\eta} &= 0 \qquad \theta_1 = \frac{\partial\theta_1}{\partial\eta} = 0 \qquad\qquad \text{on} \quad \eta = 0 \\ \frac{\partial\theta_0}{\partial\eta} &\to 1 \qquad\quad \frac{\partial\theta_1}{\partial\eta} \to 0 \qquad \text{exponentially as} \quad \eta \to \infty. \end{aligned}\right\} \tag{3.4}$$

Here we are interested in the solution in the large-$\bar{\xi}$ limit, in order to provide upstream boundary conditions for the receptivity region $\xi = O(1)$. In this limit, the mean flow is given by (2.6) and the unsteady perturbation takes the form,

$$\left.\begin{aligned} \theta_0 &\sim H_0(\eta) + \frac{\ln(\bar{\xi}^2)}{\bar{\xi}^2}H_3(\eta) + \frac{1}{\bar{\xi}^2}H_4(\eta) + O(\bar{\xi}^{-\gamma_2}), \\ \theta_1 &\sim \bar{\xi}^2\widehat{H}_0(\eta) + \ln(\bar{\xi}^2)\widehat{H}_3(\eta) + \widehat{H}_4(\eta) + O(\bar{\xi}^{(2-\gamma_2)}), \end{aligned}\right\} \tag{3.5}$$

where we have adopted this rather unusual labelling notation in order to retain consistency with the notation used in §4. The set of functions $H_i(\eta)$ and $\widehat{H}_i(\eta)$ satisfy

$$\left.\begin{aligned} \mathcal{G}_0(H_0) &= 0, & \mathcal{G}_{-2}(\widehat{H}_0) &= \mathrm{i}(1-H_0'), \\ \mathcal{G}_2(H_3) &= \mathcal{R}^{(3)}_{2,1}(H_0), & \mathcal{G}_0(\widehat{H}_3) &= -\mathrm{i}H_3' + \mathcal{R}^{(3)}_{0,3}(\widehat{H}_0), \\ \mathcal{G}_2(H_4) &= -2 - \mathcal{R}^{(4)}_{2,1}(H_0) & \mathcal{G}_0(\widehat{H}_4) &= \mathrm{i}(1 - H_0' - H_4') - \mathcal{R}^{(4)}_{0,3}(\widehat{H}_0) \\ &\quad + 2F'H_3' - 2F''H_3, & &\quad + 2F'\widehat{H}_3' - 2F''\widehat{H}_3, \end{aligned}\right\} \tag{3.6}$$

subject to boundary conditions

$$\left.\begin{aligned} H_i = H_i' &= 0, \qquad \widehat{H}_i = \widehat{H}_i' = 0, \qquad \text{on} \quad \eta = 0, \\ H_0' \to 1, \quad H_{i\geq 1}' &\to 0, \qquad\quad \widehat{H}_i' \to 0, \qquad \text{as} \quad \eta \to \infty, \end{aligned}\right\} \tag{3.7}$$

where the decay is exponential as $\eta \to \infty$. Here the operator $\mathcal{G}_\gamma$ is defined in (2.9) and the operators $\mathcal{R}^{(i)}_{\beta,\gamma}$ are defined in the Appendix. As was noted in §2, $\mathcal{G}_2$ has an eigensolution (i.e. a solution of $\mathcal{G}_2(H) = 0$ with homogeneous boundary conditions). Thus H_3 and H_4 can not be determined entirely by the large-$\bar{\xi}$ asymptotic analysis, but require knowledge of the full solution in the nose region. However, for the symmetric case considered in this section, the leading-order term in the small-S expansion can be determined exactly in terms of the steady flow (Lighthill 1954). In the notation of the present paper this gives the quasi-steady solution as $\theta_0 = \frac{1}{2}(\eta\phi_\eta + \phi)$ and hence,

$$H_0 = \tfrac{1}{2}(\eta F' + F), \qquad H_3 = \tfrac{1}{2}(\eta\overline{G}_1' + \overline{G}_1), \qquad H_4 = \tfrac{1}{2}(\eta\overline{G}_2' + \overline{G}_2), \tag{3.8}$$

where $\overline{G}_1(\eta)$, $\overline{G}_2(\eta)$ are defined in (2.10, 2.11). Solutions for $\widehat{H}_i$ are obtained using a fourth-order Runge-Kutta method, shooting from $\eta = 0$ and using the requirement of exponential decay as $\eta \to \infty$.

It is clear from (3.5) that the small-S expansion (3.1) breaks down when $S\bar{\xi}^2 = O(1)$, which is to be expected since when $\xi = O(1)$ we have reached the receptivity regime where unsteadiness enters at leading order. Within the receptivity region, we are interested only in the coefficient of the first eigensolution. We therefore anticipate the large-ξ form (2.16) by setting $\psi = \xi w(\xi,\eta)\mathrm{e}^{-\lambda\xi^3/3}$, where $\lambda = \mathrm{e}^{-\frac{1}{4}\mathrm{i}\pi}/(\rho_1^{3/2}U_0')$ as before. From (2.19a), w is given by

$$\left.\begin{aligned} \mathcal{N}_s(w) &= \left[\mathrm{i}(S+\xi^2) - \frac{2S}{S+\xi^2}\right]\mathrm{e}^{\lambda\xi^3/3}, \\ \mathcal{N}_s(w) \equiv w_{\eta\eta\eta} + [\phi + \xi\phi_\xi]w_{\eta\eta} + \left[i(S+\xi^2) - \xi\phi_{\eta\xi} + \left(\lambda\xi^3 - \frac{2S}{S+\xi^2}\right)\phi_\eta\right]w_\eta & \\ +(1-\lambda\xi^3)\phi_{\eta\eta}w + \xi(\phi_{\eta\eta}w_\xi - \phi_\eta w_{\eta\xi}). & \end{aligned}\right\} \tag{3.9}$$

Using the large-$\bar{\xi}$ form of ϕ (2.6), we see that the coefficients which appear in $\mathcal{N}_s(w)$ involve terms in $(\xi^2/S)^{-1}\ln(\xi^2/S)$ and $(\xi^2/S)^{-1}$, and hence we can expand $\mathcal{N}_s$ as an asymptotic series in S,

$$\mathcal{N}_s(w) \sim \mathcal{N}^{(0)}_{0,1}(w) + S\ln S\mathcal{N}^{(3)}_{2,1}(w) + S\mathcal{N}^{(4)}_{2,1}(w) + O(S^{\gamma_2/2}), \tag{3.10}$$

where the partial differential operators $\mathcal{N}^{(i)}_{\beta,\gamma}(w)$ are defined in the Appendix. Now writing

$$w(\xi,\eta;S) \sim w_0 + S\ln S w_3 + S w_4 + O(S^{\gamma_2/2}), \tag{3.11}$$

and expanding the right side of (3.9), we obtain a set of equations governing the evolution of $w_i(\xi,\eta)$,

$$\left.\begin{aligned} \mathcal{N}^{(0)}_{0,1}(w_0) &= \mathrm{i}\xi^2\mathrm{e}^{\lambda\xi^3/3}, \\ \mathcal{N}^{(0)}_{0,1}(w_3) &= -\mathcal{N}^{(3)}_{2,1}(w_0), \\ \mathcal{N}^{(0)}_{0,1}(w_4) &= (\mathrm{i} - 2/\xi^2)\mathrm{e}^{\lambda\xi^3/3} - \mathcal{N}^{(4)}_{2,1}(w_0). \end{aligned}\right\} \tag{3.12}$$

Matching back to (3.5) we see that as $\xi \to 0$,

$$\left.\begin{aligned} w_0 &\sim H_0 + \xi^2 \widehat{H}_0, \\ w_3 &\sim -\frac{1}{\xi^2} H_3 - \widehat{H}_3, \\ w_4 &\sim \frac{\ln(\xi^2)}{\xi^2} H_3 + \frac{1}{\xi^2} H_4 + \ln(\xi^2)\widehat{H}_3 + \widehat{H}_4. \end{aligned}\right\} \tag{3.13}$$

Thus we write

$$\left.\begin{aligned} w_0 &= \mathrm{e}^{\lambda\xi^3/3} H_0 + \xi^2 q_0, \\ w_3 &= -\frac{1}{\xi^2}\mathrm{e}^{\lambda\xi^3/3} H_3 + q_3, \\ w_4 &= -\ln(\xi^2) w_3 + \frac{1}{\xi^2}\mathrm{e}^{\lambda\xi^3/3} H_4 + q_4, \end{aligned}\right\} \tag{3.14}$$

and it can be shown after some algebraic manipulation that

$$\left.\begin{aligned} \mathcal{N}^{(0)}_{-2,3}(q_0) &= \mathrm{i}\mathrm{e}^{\lambda\xi^3/3}(1 - H_0'), \\ \mathcal{N}^{(0)}_{0,1}(q_3) &= \mathrm{i}\mathrm{e}^{\lambda\xi^3/3} H_3' - \overline{\mathcal{N}}^{(3)}_{0,3}(q_0), \\ \mathcal{N}^{(0)}_{0,1}(q_4) &= \mathrm{i}\mathrm{e}^{\lambda\xi^3/3}(1 - H_0' - H_4') - \mathrm{i}\xi^2 q_0' - \overline{\mathcal{N}}^{(4)}_{0,3}(q_0) + 2F'' q_3 - 2F' q_3', \end{aligned}\right\} \tag{3.15}$$

where q_i' denotes the partial derivative of $q_i(\xi, \eta)$ with respect to η. From (3.13), the functions q_i satisfy initial conditions

$$q_0(0, \eta) = \widehat{H}_0, \qquad q_3(0, \eta) = -\widehat{H}_3(\eta), \qquad q_4(0, \eta) = \widehat{H}_4(\eta), \tag{3.16}$$

and homogeneous boundary conditions, $q_i(\xi, 0) = q_i'(\xi, 0) = 0$, $q_i' \to 0$ exponentially as $\eta \to \infty$. The differential operators $\overline{\mathcal{N}}^{(i)}_{\beta,\gamma}$, related to the operators $\mathcal{N}^{(i)}_{\beta,\gamma}$, are defined in the Appendix. Thus the evolution of the $O(S^0)$, $O(S \ln S)$ and $O(S)$ components of the unsteady flow has been cast in a form suitable for accurate numerical computation. Numerical solutions of (3.15) are discussed in §5.

4. Receptivity to antisymmetric forcing

At first sight, the analysis of the receptivity in the anti-symmetric case appears to follow very similarly to the symmetric case. However, a subtle difference is seen in the structure of the solution. Motivated by the anti-symmetric forcing (2.19*b*), we write the small-S expansion of the unsteady perturbation in the nose region, $\bar{\xi} = O(1)$, as

$$\psi_a = \psi_0(\bar{\xi}, \eta) + S\,\psi_1(\bar{\xi}, \eta) + O(S^2). \tag{4.1}$$

The perturbation is again quasi-steady at leading order in the nose region, with

$$\left.\begin{aligned} \mathcal{M}_a(\psi_0) &= \frac{\bar{\xi}^2 - 1}{\bar{\xi}^2 + 1}, \\ \mathcal{M}_a(\psi_1) &= \mathrm{i}(1 + \bar{\xi}^2)\big(1 - (\psi_0)_\eta\big), \end{aligned}\right\} \tag{4.2}$$

where

$$\mathcal{M}_a(p) \equiv \mathcal{M}_s(p) + \phi_\eta p_\eta - \phi_{\eta\eta} p. \tag{4.3}$$

However, in contrast to the symmetric case, the large-$\bar{\xi}$ limit for the unsteady flow now takes the form

$$\left.\begin{aligned}\psi_0 &\sim J_0(\eta) + \frac{\ln(\bar{\xi}^2)}{\bar{\xi}} J_1(\eta) + \frac{1}{\bar{\xi}} J_2(\eta) + \frac{\ln(\bar{\xi}^2)}{\bar{\xi}^2} J_3(\eta) + \frac{1}{\bar{\xi}^2} J_4(\eta) + O(\bar{\xi}^{(1-\gamma_2)}) \\ \psi_1 &\sim \bar{\xi}^2 \widehat{J}_0(\eta) + \bar{\xi} \ln(\bar{\xi}^2) \widehat{J}_1(\eta) + \bar{\xi} \widehat{J}_2(\eta) + \ln(\bar{\xi}^2) \widehat{J}_3(\eta) + \widehat{J}_4(\eta) + O(\bar{\xi}^{(3-\gamma_2)})\end{aligned}\right\} \tag{4.4}$$

where the functions $J_i(\eta)$ and $\widehat{J}_i(\eta)$ satisfy

$$\left.\begin{aligned}&\mathcal{G}_1(J_0)=1, && \mathcal{G}_{-1}(\widehat{J}_0)=\mathrm{i}(1-J_0'), \\ &\mathcal{G}_2(J_1)=0, && \mathcal{G}_0(\widehat{J}_1)=-\mathrm{i}J_1', \\ &\mathcal{G}_2(J_2)=2F'J_1' - 2F''J_1, && \mathcal{G}_0(\widehat{J}_2)=-\mathrm{i}J_2' + 2F'\widehat{J}_1' - 2F''\widehat{J}_1, \\ &\mathcal{G}_3(J_3)=\mathcal{R}^{(3)}_{3,0}(J_0), && \mathcal{G}_1(\widehat{J}_3)=-\mathrm{i}J_3' + \mathcal{R}^{(3)}_{1,2}(\widehat{J}_0), \\ &\mathcal{G}_3(J_4)=-2 - \mathcal{R}^{(4)}_{3,0}(J_0) && \mathcal{G}_1(\widehat{J}_4)=\mathrm{i}(1-J_0'-J_4') - \mathcal{R}^{(4)}_{1,2}(\widehat{J}_0) \\ &\qquad +2F'J_3' - 2F''J_3, && \qquad +2F'\widehat{J}_3' - 2F''\widehat{J}_3,\end{aligned}\right\} \tag{4.5}$$

with boundary conditions

$$\left.\begin{aligned}J_i = J_i' = 0 \qquad \widehat{J}_i = \widehat{J}_i' = 0 \qquad &\text{on} \quad \eta = 0 \\ J_0' \to 1, \quad J_{i\geq 1}' \to 0 \qquad \widehat{J}_i' \to 0 \qquad &\text{as} \quad \eta \to \infty.\end{aligned}\right\} \tag{4.6}$$

Compared to the expansion for the symmetric case (3.5), the additional terms in $\ln(\bar{\xi}^2)/\bar{\xi}$ and $1/\bar{\xi}$ are included in the large-$\bar{\xi}$ expansion of ψ_0 because the operator $\mathcal{G}_2$ possesses an eigensolution. Thus $J_1(\eta) = P_1(\eta F' - F)$, where the numerical constant P_1 can be determined from the solvability condition for J_2. As noted in §2, the Blasius function F is the solution to the adjoint of $\mathcal{G}_2$ and we see that

$$\begin{aligned}0 &= \int_0^\infty F(F'J_1' - F''J_1)\,\mathrm{d}\eta = 2P_1 \int_0^\infty F^2 F''\,\mathrm{d}\eta \\ &= P_1.\end{aligned} \tag{4.7}$$

Hence $J_1 \equiv 0$ and it follows that $\widehat{J}_1 \equiv 0$, and $J_2(\eta) = P_2(\eta F' - F)$, where P_2 is a numerical constant. Solutions to the set of equations (4.5) are obtained by shooting, as described in §3, but the value of the constant P_2 in the expression for J_2 can only be determined by comparison with numerical solutions of ψ_0 obtained by integrating (4.2) forward from $\bar{\xi} = 0$. Comparing the computed wall shear $\psi_0''(\bar{\xi}, 0)$, with the asymptotic form (4.4) gives

$$P_2 \approx 6.07, \tag{4.8}$$

but accurate extrapolation is difficult due to the presence of higher-order terms in the expansion (4.4). The numerical results suggest that the coefficients of these terms are in fact relatively large. This is discussed further in §5.

In the receptivity region $\xi = O(1)$ where unsteadiness enters at leading order, we again

anticipate the large-ξ form of the eigensolution by setting $\psi_a = v\mathrm{e}^{-\lambda\xi^3/3}$. The function $v(\xi,\eta;S)$ then satisfies

$$\left.\begin{aligned}\mathcal{N}_a(v) &= \left[\mathrm{i}(S+\xi^2) - \frac{S-\xi^2}{S+\xi^2}\right]\mathrm{e}^{\lambda\xi^3/3},\\ \mathcal{N}_a(v) &\equiv \mathcal{N}_s(v) + \phi_\eta v_\eta - \phi_{\eta\eta} v,\end{aligned}\right\} \tag{4.9}$$

where $\mathcal{N}_s(v)$ was defined in §3. As for the symmetric case, we expand the operator as an asymptotic series in S,

$$\mathcal{N}_a(v) \sim \mathcal{N}^{(0)}_{1,0}(v) + S\ln S\mathcal{N}^{(3)}_{3,0}(v) + S\mathcal{N}^{(4)}_{3,0}(v) + O(S^{\gamma_2/2}), \tag{4.10}$$

but in this case, guided by the asymptotic form (4.4) in the nose region, we expand $v(\xi,\eta;S)$ as

$$v \sim v_0 + S^{1/2}v_2 + S\ln S v_3 + Sv_4 + O(S^{(\gamma_2-1)/2}). \tag{4.11}$$

Matching back to the nose region then suggests that we set

$$\left.\begin{aligned}v_0 &= \mathrm{e}^{\lambda\xi^3/3}J_0 + \xi^2 p_0,\\ v_2 &= \frac{1}{\xi}\mathrm{e}^{\lambda\xi^3/3}J_2 + \xi p_2,\\ v_3 &= -\frac{1}{\xi^2}\mathrm{e}^{\lambda\xi^3/3}J_3 + p_3,\\ v_4 &= -\ln(\xi^2)v_3 + \frac{1}{\xi^2}\mathrm{e}^{\lambda\xi^3/3}J_4 + p_4.\end{aligned}\right\} \tag{4.12}$$

This finally leads to the set of equations

$$\left.\begin{aligned}\mathcal{N}^{(0)}_{-1,2}(p_0) &= \mathrm{i}\mathrm{e}^{\lambda\xi^3/3}(1-J_0'),\\ \mathcal{N}^{(0)}_{0,1}(p_2) &= -\mathrm{i}\mathrm{e}^{\lambda\xi^3/3}J_2',\\ \mathcal{N}^{(0)}_{1,0}(p_3) &= \mathrm{i}\mathrm{e}^{\lambda\xi^3/3}J_3' - \overline{\mathcal{N}}^{(3)}_{1,2}(p_0),\\ \mathcal{N}^{(0)}_{1,0}(p_4) &= \mathrm{i}\mathrm{e}^{\lambda\xi^3/3}(1-J_0'-J_4') - i\xi^2 p_0' - \overline{\mathcal{N}}^{(4)}_{1,2}(p_0) + 2F''p_3 - 2F'p_3',\end{aligned}\right\} \tag{4.13}$$

with initial conditions

$$p_0(0,\eta) = \widehat{J}_0, \qquad p_2(0,\eta) = \widehat{J}_2, \qquad p_3(0,\eta) = -\widehat{J}_3(\eta), \qquad p_4(0,\eta) = \widehat{J}_4(\eta), \tag{4.14}$$

and the homogeneous boundary conditions, $p_i(\xi,0) = p_i'(\xi,0) = 0$, $p_i' \to 0$ exponentially as $\eta \to \infty$. As in §3, we use p_i' to denote the partial derivative of $p_i(\xi,\eta)$ with respect to η. Numerical solutions to this set of equations are discussed in the next section.

5. Numerical Results

Having obtained expressions for the evolution of the unsteady flow in the form of an asymptotic expansion for small S, we now carry out the numerical integration required to obtain the corresponding asymptotic expansion for the receptivity coefficient $C_1(S)$. As explained in HK1, in order to reliably extract the coefficient $C_1(S)$ of the first asymptotic eigensolution from the numerical results, it is necessary to carry out the integration in the

complex-ξ plane, in the region $-5\pi/12 < \arg(\xi) < -\pi/12$ where the first eigensolution of the LUBLE exhibits exponential growth and is the dominant component of the solution at large ξ. The sets of equations (3.15) and (4.13) were integrated forward in ξ, from $\xi = 0$ to $|\xi| = 10$ using a Keller Box scheme (Keller & Cebeci 1970), with $\arg(\xi)$ chosen as either $-\pi/3$ or $-\pi/4$ to ensure the dominance of the first eigensolution.

For large ξ, the first asymptotic eigensolution is given by (2.16). Expanding the expression for the first eigensolution (2.16) for small S, and writing the receptivity coefficient, $C_a(S)$ or $C_s(S)$, as an expansion for small S,

$$C(S) \sim C(0)\big(1 + c_2 S^{1/2} + c_3 S \ln S + c_4 S + \ldots\big), \tag{5.1}$$

we see that as $\xi \to \infty$ in the region of the complex plane of interest,

$$\begin{aligned}\psi \sim \psi_0\big(1 + c_2 S^{1/2} + [c_3 - \lambda A_1 \xi] S \ln S + \\ [c_4 + \tau_1 \ln(\xi^2/2) - \lambda\xi(2A_1 + \tfrac{3}{2} - B_1 - A_1 \ln(\xi^2))] S\big),\end{aligned} \tag{5.2}$$

where ψ_0 is the first eigensolution for the flat-plate case (Goldstein 1983). The coefficients $C(0)$, c_2, c_3 and c_4 can then be obtained by comparison with the numerical solution either at the outer edge of the boundary layer or at the wall.

For the symmetric case clearly $c_2^{(s)} = 0$, while $C_s(0)$, $c_3^{(s)}$, $c_4^{(s)}$ are extracted from the limiting forms

$$\left.\begin{aligned} &w_0 \sim C_s(0)\,\big(\xi^2/2\big)^{\tau_1^{(0)}}\,[1 + O(\xi^{-1})], \\ &\frac{w_3}{w_0} \sim c_3^{(s)} - \lambda A_1 \xi, \\ &\frac{w_4}{w_0} \sim c_4^{(s)} + \tau_1^{(1)} \ln(\xi^2/2) - \lambda\xi(2A_1 + \tfrac{3}{2} - B_1 - A_1 \ln(\xi^2)), \end{aligned}\right\} \tag{5.3}$$

as $\eta, \xi \to \infty$. The evolution of w_0 is the flat-plate case described by Goldstein and gives

$$C_s(0) = -0.441 + 0.841\,\mathrm{i} \tag{5.4}$$

as the receptivity coefficient for a flat plate, in agreement with earlier results (Goldstein *et al.* 1983; Heinrich & Kerschen 1989). Using $\arg(\xi) = -\pi/4$, the corrections taking account of small nose radius effects are calculated to be

$$c_3^{(s)} \approx 0, \qquad c_4^{(s)} \approx 3.12 - 2.37\,\mathrm{i}. \tag{5.5}$$

Integration using $\arg(\xi) = -\pi/3$ gives a difference of less than 2% in the estimate for $c_4^{(s)}$. Hence

$$\left.\begin{aligned} &\mathrm{Re}(C_s(S)) \sim -0.441 + 0.62\,S + O(S^{\alpha_1}) \\ &\mathrm{Im}(C_s(S)) \sim \ \ 0.841 + 3.67\,S + O(S^{\alpha_1}), \quad \alpha_1 = \tfrac{1}{2}\gamma_2 \approx 1.887. \end{aligned}\right\} \tag{5.6}$$

In figure 2 asymptotic results (5.5) are compared with the results of the full integration for small-S presented in HK1. To make the comparisons as clear as possible, we plot the perturbation from the flat plate result $f(S) = \big(C(S) - C(0)\big)/C(0)$ as a function of S and compare this with the asymptotic form (5.1). In figure 2*a* and *b*, comparisons are made for the symmetric case, making it clear that the leading-order behaviour for the symmetric receptivity coefficient is indeed described by (5.6). The small discrepancy between numerical results and asymptotic theory is likely to be due either to numerical

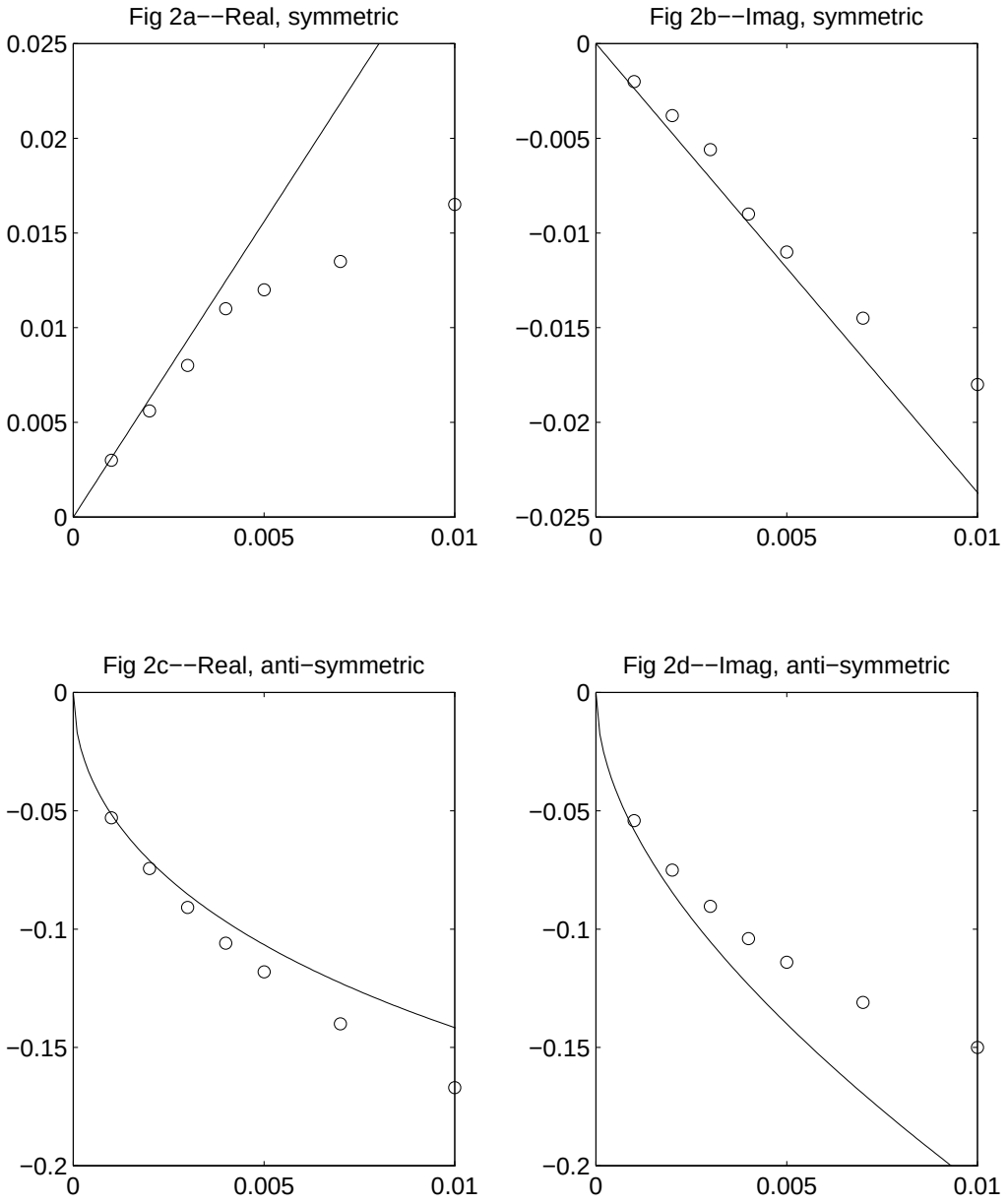

FIGURE 2. Comparison of numerical and asymptotic results for the receptivity due to symmetric and anti-symmetric disturbances. Numerical results for the perturbation $f(S) = \big(C(S) - C(0)\big)/C(0)$ (see text) are denoted by $\circ$, asymptotic theory is marked by the solid line. Results for $\mathrm{Re}(f_s)$ and $\mathrm{Im}(f_s)$ are illustrated in (a) and (b), respectively, and $\mathrm{Re}(f_a)$ and $\mathrm{Im}(f_a)$ are illustrated in (c) and (d).

uncertainty in extrapolating $C(S)$ from large-ξ calculations (as explained in HK1), or to the higher-order terms in (5.6).

For the anti-symmetric case,

$$\left.\begin{aligned} &v_0 \sim C_a(0)\xi\left(\xi^2/2\right)^{\tau_1^{(0)}}\,[1+O(\xi^{-1})],\\ &\frac{v_2}{v_0}\sim c_2^{(a)},\\ &\frac{v_3}{v_0}\sim c_3^{(a)}-\lambda A_1\xi,\\ &\frac{v_4}{v_0}\sim c_4^{(a)}+\tau_1^{(1)}\ln(\xi^2/2)-\lambda\xi(2A_1+\tfrac{3}{2}-B_1-A_1\ln(\xi^2)), \end{aligned}\right\} \tag{5.7}$$

as $\eta,\xi\to\infty$. Comparing these large-ξ asymptotic forms with numerical results gives

$$C_a(0)\approx -5.33+1.66\,\mathrm{i}, \tag{5.8}$$

as the flat-plate solution, with small-S corrections

$$c_2^{(a)}\approx -1.728-1.728\,\mathrm{i}, \qquad c_3^{(a)}\approx 0, \qquad c_4^{(a)}\approx 3.12-3.57\,\mathrm{i}. \tag{5.9}$$

Again there is no significant difference in these results if $\arg(\xi)$ is varied. Hence

$$\left.\begin{aligned} &\mathrm{Re}(C_a(S))\sim -5.33+12.08\,S^{1/2}-10.7\,S+O(S^{\alpha_2})\\ &\mathrm{Im}(C_a(S))\sim\ \ 1.66+\ 6.34\,S^{1/2}+24.2\,S+O(S^{\alpha_2}),\quad \alpha_2=\frac{1}{2}(\gamma_2-1)\approx 1.387 \end{aligned}\right\} \tag{5.10}$$

In figure 2c and d the asymptotic results (5.9) are compared with the results of the full integration for small-S presented in HK1. It is clear that the coefficient of the $S^{\frac{1}{2}}$ term in (5.10) is correct. While it is not possible to be certain from these results that the $O(S)$ terms are also correct, the divergence of the asymptotic results from numerical results arises at similar values of S to the symmetric case, when the $O(S)$ terms were seen to be correct. In addition, it should be noted that the next higher order term in (5.10) is $O(S^{\alpha_2})$, $\alpha_2\approx 1.387$ which is very close in magnitude to the $O(S)$ term retained. Comparison of numerical results and asymptotic solutions in the nose region suggests that the coefficient of the next term in the expansion (4.4) is fairly large, further suggesting that the $O(S^{\alpha_2})$ in (5.10) is indeed significant, even for small S. Hence figure 2c and d shows that the asymptotic form (5.10) is at least consistent with numerical results.

The absence of any $S\ln S$ term in the expansions of the symmetric and anti-symmetric receptivity coefficients is somewhat surprising. However, further insight can be gained by considering the case $\arg(\xi)=-\pi/4$ in more detail. In this special case, the operators $\mathcal{N}^{(0)}$, $\overline{\mathcal{N}}^{(3)}$ and $\overline{\mathcal{N}}^{(4)}$ defined in the Appendix are real. Noting that the set of functions $\widehat{H}(\eta)$ are purely imaginary, equations (3.15) show that the functions $q_i(\xi,\eta)$ are also wholly imaginary. Hence in the limit $|\xi|\to\infty$, w_3/w_0 is imaginary and $\mathrm{Re}(c_3^{(s)})=0$. That is, if there is a $S\ln S$ term in the small-S expansion of $C_s(S)$, then it is wholly imaginary. Furthermore, we can show from the large-ξ limit of w_4/w_0, that

$$\mathrm{Re}(c_4^{(s)})=-\frac{\pi}{2}\mathrm{Im}(\tau_1^{(1)}+c_3^{(s)}). \tag{5.11}$$

These results are in agreement with the numerical results. The same results also apply to the anti-symmetric case. Further consideration of the large-ξ limit of w_0 and v_0 for $\arg(\xi)=-\pi/4$ proves that

$$\arg\big(C_s(0)\big)=-\frac{\pi}{2}(1+\tau_1^{(0)}), \qquad \arg\big(C_a(0)\big)=-\frac{\pi}{2}(\tfrac{1}{2}+\tau_1^{(0)}) \tag{5.12}$$

which confirms the numerics, and also explains the $\pi/4$ difference in phase between flat-plate receptivity coefficients for symmetric and anti-symmetric forcing noted in HK1.

6. Summary

In §5, the small-S expansions of the real and imaginary parts of the receptivity coefficients for symmetric and anti-symmetric forcing were compared with numerical results. From a practical standpoint, the most important quantity is the modulus of the receptivity coefficient, since it is the variation of this that is likely to influence the position of the transition point. In figure 3, the asymptotic prediction for the modulus of the receptivity coefficient is compared to numerical results, for symmetric and anti-symmetric forcing. For oblique acoustic waves ($\theta \neq 0$), the coefficient κ_a in (2.18) is often large compared to κ_s (see HK1). Moreover, as $S \to 0$ the anti-symmetric receptivity coefficient C_a is approximately five times larger than C_s, the symmetric receptivity coefficient. Hence $C_a(S)$ is much more important than $C_s(S)$ in determining the behaviour of the total receptivity coefficient $C_1(S)$. In this paper, we have shown that $C_a(S)$ has a singular structure for small S, varying as $S^{\frac{1}{2}}$, so that small changes in this parameter have a significant influence on the receptivity. Moreover, the exact form of this leading-order behaviour has been accurately calculated. The rather small range of validity of the asymptotic expansions at first appears somewhat disappointing. However, numerical results show that the maximum receptivity occurs for small S and hence the behaviour in this limit is of most interest for practical applications. For $S < 0.005$, excellent agreement is seen between asymptotic theory and numerical results, so in this parameter range the asymptotic expansions developed in this paper are of quantitative as well as qualitative value.

The small-S limit is also of interest when considering the experimental results of Saric *et al.* (1995). In these wind-tunnel tests, a leading edge consisting of a machined super-ellipse of either 1:20 or 1:40 aspect ratio is attached to a flat plate. By considering a super-ellipse profile rather than an ellipse for the leading-edge section, localised receptivity due to a discontinuity in surface curvature at the join with the flat plate (Goldstein 1985) is eliminated. The region of dominant receptivity should then be the leading edge. Measurements were made for free-stream speeds $8\mathrm{ms}^{-1} < U < 21\mathrm{ms}^{-1}$, corresponding to nose radius Reynolds numbers $Re_n = Ur_n/\nu$ in the range $130 < Re_n < 670$, consistent with the assumption $Re_n \gg 1$ used in our analysis. Acoustic forcing at non-dimensional frequencies in the range $30 \times 10^{-6} < \epsilon^6 < 90 \times 10^{-6}$ was considered, leading to a Strouhal number range $0.004 < S < 0.060$. Our small-S theory is clearly relevant to the lower end of this Strouhal number range. The results of the present analysis show that, despite the small values of the nose radius in these experiments, there can be significant departures from the flat-plate results. Many of the detailed measurements of Saric *et al.* are for a Strouhal number of 0.01. For this value of S, symmetric disturbances lead to receptivity 2% greater than the flat plate value, but for anti-symmetric forcing there is a 15% reduction compared to the flat-plate result. As noted earlier, despite the small numerical values of S, by $S = 0.01$ the computed value of the receptivity coefficient has already begun to diverge from the asymptotic results.

For leading-edge receptivity, various measures of receptivity can be considered. We have chosen to define C_1, the coefficient of the first Lam–Rott asymptotic eigenfunction, as the 'receptivity coefficient'. Alternative definitions of receptivity level that have been considered in computations and experiments are values based on the Tollmien–Schlichting wave amplitude at the lower neutral-stability point (branch I), or on an extrapolation of the Tollmien–Schlichting wave amplitude back to the leading edge. Extrapolation of

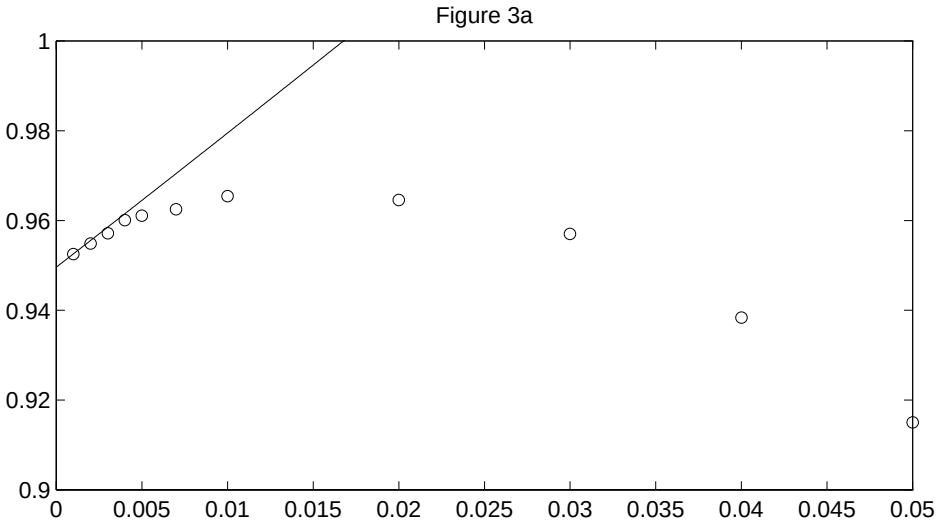

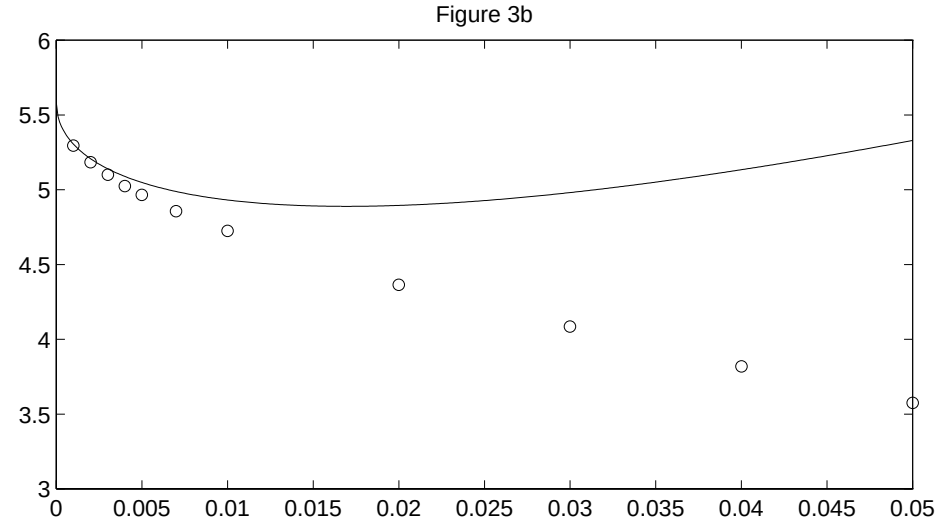

FIGURE 3. Comparison of numerical and asymptotic results for the modulus of the receptivity coefficient for *(a)* symmetric forcing and *(b)* anti-symmetric forcing. Numeric results are denoted by ∘, asymptotic theory is marked by the solid line.

the Tollmien–Schlichting wave amplitude back to the leading edge is not advisable, since the Tollmien–Schlichting wave is not a valid solution of the disturbance equations near the leading edge. In fact, in extrapolating back to the leading edge the slowly varying amplitude $A(\xi)$ multiplying the mode-shape function of the Tollmien–Schlichting wave should be considered, and $A(\xi)$ becomes infinite at the leading edge, the streamwise velocity fluctuation behaving as $\xi^{2\tau_1}$ where $\tau_1 = \tau_1^{(0)} + S\tau_1^{(1)}$ is given by (2.16).

A receptivity level defined in terms of the Tollmien–Schlichting wave amplitude at the lower branch neutral-stability point does allow easy comparison with experiments or computations, but has the disadvantage that the results depend on the frequency and

Reynolds number, making presentation of the results much less compact. However, there is a need to relate receptivity levels defined in terms of C_1 to levels expressed in terms of branch I amplitudes. In the asymptotic theory, this is achieved by developing the asymptotic expression for the Tollmien–Schlichting wave in the OSE region and matching this expression to the first generalised Lam–Rott asymptotic eigensolution (2.16). This procedure is discussed by Goldstein (1983) for the flat-plate case, and the extension to non-zero S is discussed briefly in HK1. However, the asymptotic analysis is quite laborious, especially for the determination of $A(\xi)$. An alternative approach is the numerical solution of the disturbance equations, using the Lam–Rott asymptotic eigensolution as a starting condition and continuing downstream to branch I.

From a theoretical standpoint, the most attractive measure of receptivity is the coefficient C_1 of the first Lam–Rott asymptotic eigenfunction. This Lam–Rott eigenfunction evolves into the unstable Tollmien–Schlichting wave farther downstream so that, when appropriate scaling factors related to the asymptotic matching of the LUBLE and OSE regions are introduced, C_1 is also the coefficient of the Tollmien–Schlichting wave. An extremely attractive feature of this receptivity measure is that C_1 is independent of the physical frequency and the (asymptotically large) Reynolds number, thus providing the receptivity results in the simplest dimensionless form. The quantity C_1 is determined by the unsteady flow behaviour upstream of the region of instability and therefore focuses on the receptivity aspect of the unsteady flow development, with less influence from the global stability properties of the flow. Also, for fixed values of the frequency and Reynolds number, variations in the receptivity coefficient C_1 with changes in the free-stream disturbance characteristics translate directly into variations in the Tollmien–Schlichting wave amplitude.

This work was supported by NASA Langley Research Center under grant NAG-1-1135 and Air Force Office of Scientific Research under grant F49620-94-1-0206.

Appendix A. Definition of the operators $\mathcal{N}^{(i)}_{\beta,\gamma}(w)$ and $\mathcal{R}^{(i)}_{\beta,\gamma}(w)$.

In §§3 and 4 a set of partial differential operators $\mathcal{N}^{(i)}_{\beta,\gamma}(w)$ are used. These are defined as

$$\left.\begin{aligned}
\mathcal{N}^{(0)}_{\beta,\gamma}(w)&=w_{\eta\eta\eta}+Fw_{\eta\eta}+\left[i\xi^2+(\beta+\lambda\xi^3)F'\right]w_\eta+(\gamma-\lambda\xi^3)F''w\\
&\qquad+\xi(F''w_\xi-F'w_{\eta\xi}),\\
\mathcal{N}^{(3)}_{\beta,\gamma}(w)&=\frac{1}{\xi^2}\overline{\mathcal{N}}^{(3)}_{\beta,\gamma}(w),\\
\mathcal{N}^{(4)}_{\beta,\gamma}(w)&=-\frac{\ln(\xi^2)}{\xi^2}\overline{\mathcal{N}}^{(3)}_{\beta,\gamma}(w)+\frac{1}{\xi^2}\overline{\mathcal{N}}^{(4)}_{\beta,\gamma}(w)+iw_\eta.
\end{aligned}\right\}\qquad(\text{A }1)$$

where

$$\left.\begin{aligned}
\overline{\mathcal{N}}^{(3)}_{\beta,\gamma}(w)&=\overline{G}_1w_{\eta\eta}-(\beta+\lambda\xi^3)\overline{G}'_1w_\eta-(\gamma-\lambda\xi^3)\overline{G}''_1w-\xi(\overline{G}''_1w_\xi-\overline{G}'_1w_{\eta\xi}),\\
\overline{\mathcal{N}}^{(4)}_{\beta,\gamma}(w)&=(2\overline{G}_1-\overline{G}_2)w_{\eta\eta}+\left((\beta+\lambda\xi^3)\overline{G}'_2-2(F'+\overline{G}'_1)\right)w_\eta\\
&\qquad+(\gamma-\lambda\xi^3)\overline{G}''_2w+\xi(\overline{G}''_2w_\xi-\overline{G}'_2w_{\eta\xi})
\end{aligned}\right\}\qquad(\text{A }2)$$

In addition, the set of differential operators $\mathcal{R}^{(i)}_{\beta,\gamma}(f)$ are used, defined by

$$\left.\begin{aligned}\mathcal{R}^{(3)}_{\beta,\gamma}(f)&=\overline{G}_1 f_{\eta\eta} - \beta\overline{G}_1' f_\eta - \gamma\overline{G}_1'' f \\ \mathcal{R}^{(4)}_{\beta,\gamma}(f)&=(2\overline{G}_1 - \overline{G}_2) f_{\eta\eta} + \left(\beta\overline{G}_2' - 2(F' + \overline{G}_1')\right) f_\eta + \gamma\overline{G}_2'' f\end{aligned}\right\} \tag{A 3}$$

so that

$$\overline{\mathcal{N}}^{(i)}_{\beta,\gamma}(e^{\lambda\xi^3/3} f(\eta)) = e^{\lambda\xi^3/3}\mathcal{R}^{(i)}_{\beta,\gamma}(f(\eta)) \tag{A 4}$$

for $i = 3, 4$.

REFERENCES

Brown, S.N. & Stewartson, K. 1973 On the propagation of disturbances in a laminar boundary layer. *Proc. Camb. Phil. Soc.* **73**, 493–514.

Goldstein, M.E. 1983 The evolution of Tollmien–Schlichting waves near a leading edge. *J. Fluid Mech.* **127**, 59–81.

Goldstein, M.E. 1985 Scattering of acoustic waves into Tollmien–Schlichting waves by small streamwise variations in surface geometry. *J. Fluid Mech.* **154**, 509–529.

Goldstein, M.E. & Hultgren, L.S. 1989 Boundary-layer receptivity to long-wave free-stream disturbances. *Ann. Rev. Fluid Mech.* **21**, 137–166.

Goldstein, M.E., Sockol, P.M. & Sanz, J. 1983 The evolution of Tollmien–Schlichting waves near a leading edge. Part 2. Numerical determination of amplitudes. *J. Fluid Mech.* **129**, 443–453.

Hammerton, P.W. & Kerschen, E.J. 1996 Boundary-layer receptivity for a parabolic leading edge. *J. Fluid Mech.* **310**, 243–267.

Heinrich, R.A.E. & Kerschen, E.J. 1989 Leading-edge boundary layer receptivity to various free-stream disturbance structures. *Z. angew. Math. Mech.* **69** 6, T596–598.

Keller, H.B. & Cebeci, T. 1970 Accurate numerical methods for boundary layer flows– I. Two-dimensional laminar flows. In *Proceedings of the Second International Conference on Numerical Methods in Fluid Mechanics* (ed. M. Holt) pp. 92–100. Springer.

Kerschen, E.J. 1990 Boundary layer receptivity theory. *Appl. Mech. Rev.* **43**, 152–157.

Lam, S.H. & Rott, N. 1960 Theory of linearized time-dependent boundary layers. *Cornell Univ. Grad. School of Aero. Engineering Rep.* AFOSR TN–60–1100.

Libby, P.A. & Fox, H. 1963 Some perturbation solutions in laminar boundary layer theory. Part 1: The momentum equation. *J. Fluid Mech.* **17**, 433–449.

Lighthill, M.J. 1954 The response of laminar skin friction and heat transfer to fluctuations in the free-stream velocity. *Proc. R. Soc. Lond.* A **224** 1–23.

Saric, W.S., Wei, W., Rasmussen, B.K. & Krutckoff, T.K. 1995 Experiments on leading-edge receptivity to sound. *AIAA 95-2253*.

Van Dyke, M.D. 1964 Higher approximations in boundary layer theory. Part 3. Parabola in uniform stream. *J. Fluid Mech.* **19**, 145–159.